PCCP

Accepted Manuscript

ROYAL SOCIETY OF CHEMISTRY

www.rsc.org/pccp

Physicochemical perspectives (aggregation, structure and dynamics) of interaction between pluronic (L31) and surfactant (SDS)

G. K. S. Prameela,[a] B. V. N. Phani Kumar,[a] A. Pan,[b] V. K. Aswal,[c*] J. Subramanian,[a] A. B. Mandal,[a*] and S. P. Moulik[b*]

[a]*Chemical Physics Laboratory and Chemical Laboratory,*

CSIR- Central Leather Research Institute, Adayar, Chennai-600020, India.

Phone: +91-44-2491-0846; Fax: +91-44-2491-2150

E-mail: abmandal@hotmail.com, abmandal@clri.res.in

[b]*Centre for Surface Science, Department of Chemistry, Jadavpur University,*

Kolkata 700032, India.

Phone: +91-33-2414-6411; Fax: +91-33-2414-6266.

E-mail: spmcss@yahoo.com

[c]*Solid State Physics Division, Bhabha Atomic Research Centre, Trombay, Mumbai- 400 085, India.*

Phone: +91-22-2559-4642; Fax: +91-22-2550-5150

E-mail: vkaswal@barc.gov.in

Physicochemical perspectives (aggregation, structure and dynamics) of interaction between pluronic (L31) and surfactant (SDS)

Abstract

The influence of water soluble nonionic tri-block copolymer PEO–PPO–PEO [poly(ethylene oxide)–poly(propylene oxide)–poly(ethylene oxide)] i.e., $E_2P_{16}E_2$ (L-31) on the microstructure and self-aggregation dynamics of anionic surfactant sodium dodecylsulfate (SDS) in aqueous solution was investigated using cloud point (CP), isothermal titration calorimetry (ITC), high resolution nuclear magnetic resonance (NMR), electron paramagnetic resonance (EPR), and small-angle neutron scattering (SANS) measurements. CP provided the thermodynamic information on the Gibbs free energy, enthalpy, entropy and heat capacity changes pertaining to phase separation of the system at elevated temperature. The ITC and NMR self-diffusion measurements helped to understand the nature of the binding isotherms of SDS in the presence of L31 in terms of the formation of mixed aggregates and free SDS micelles in solution. EPR analysis provided the micro viscosity of the spin probe 5-DSA in terms of rotational correlation time. The SANS study indicated the presence of prolate ellipsoidal mixed aggregates, whose size increased with increasing addition of L31. At a large [L31], SANS also revealed the progressive decreasing size of the ellipsoidal mixed aggregates of SDS-L31 into nearly globular forms with increasing SDS addition. Wrapping of the spherical SDS micelles by L31 was also corroborated from ^{13}C NMR and SANS measurements.

1. Introduction

Polymer-surfactant interaction has been a fascinating topic from the view points of biological and commercial applications apart from academic interest. The observation that the aqueous solutions of polymer bound surfactant micelles contain higher solubilization power as well as viscosity compared to either pure surfactant or pure polymer, have favored their industrial impotance. The fundamental knowledge of polymer-surfactant interaction has enriched the formulations of paints and coatings, cosmetics, tertiary oil recovery, etc.[1,2]

The tri-block copolymers of the type $E_mP_n E_m$ (commercially known as pluronics) are non-ionic surfactants that mimic the micellization of conventional surfactants. The self- aggregation and surface activity of block copolymers (BCs) are highly sensitive to temperature, concentration, additives, composition ratio (PPO/PEO or polypropylene oxide/polyethylene oxide), etc. compared to conventional surfactants.[2,3] It is not surprising that BCs are now becoming nano-carriers in controlled drug delivery, as well as templates for the preparation of nano-structured materials.[4] To a great extent, polymer–surfactant interactions are mainly governed by hydrophobic and electrostatic interactions.[4,5]

It is known that copolymer hydrophobicity plays an important role on the self-aggregation and microstructure of a conventional surfactant. The copolymers of the type $E_mP_nE_m$ having higher (PPO/PEO) ratio are known to exhibit non-spherical micelles with increasing temperature and concentration.[3] In this context , the hydrophobic triblock copolymer $E_2P_{16}E_2$ (L31) was chosen. In an earlier study, the CMC and related information on L31 was reported.[6] The density and heat capacity measurements of aqueous L31,[7] and L31 in the presence of SDS[8] revealed the thermodynamic properties and the mechanism of binding of L31 with the amphiphile. In fact, the studies of Lopes and Loh suggested some other ordered phases

than the micellar phase in Pluronics (including L31).[6] However, to the best of our knowledge, the structural evaluation of the pluronics in the presence of surfactants in solution has been found to be nonexplored. In the present work, a detailed systematic physicochemical investigation on the ternary mixtures of L31/SDS/Water as a function of concentrations of both SDS and L31 has been made. The fundamentals of their self- and mixed aggregation, phase separation (clouding) microstructure, aggregate dynamics (diffusion), aggregate geometry, composition and ionization have been estimated, presented and discussed. Such an elaborate study on a hydrophobic pluronic like L31 and a conventional ionic surfactant like SDS has been rarely found in literature.

The study has revealed the existence of mixed aggregates and free surfactant micelles in solution; also the onset of critical aggregation concentration (CAC) for the formation of polymer-induced small micelles, and afterwards the formation of the extended CMC (or CMC_e) of formation of free SDS micelles in solution have been understood. The CP, ITC, EPR and NMR measurements have presented reliable information of CAC and CMC_e and the thermodynamic parameters like standard Gibbs free energy, enthalpy, and entropy changes of the underlying processes.[4,5] The micro-viscosity of the assemblies under investigation was monitored by the EPR measurements,[9] whereas NMR parameters (chemical shift, spin-relaxation and self-diffusion) provided information of microstructure and dynamics at the nano structural level.[10-22] The geometry of the assemblies, their aggregation number and counter-ion dissociation have been assessed from SANS[23] measurements.

2. Experimental Section

Materials

The triblock co-polymer $E_2P_{16}E_2$ (where E and P denote ethylene oxide and propylene oxide, respectively) commercially known as Pluronic L31[6,8] of molecular weight 1100**,** was obtained from Aldrich, and used as received. L31 is a water-soluble amphiphilic triblock co-polymer, which behaves like a non-ionic surfactant. Sodium dodecylsulfate (SDS) was received from Aldrich and used after purification (details given elsewhere).[22] The NMR reference standards 2,2-dimethyl-2-silapentane-5-sulfonate sodium salt (Z97%, DSS) and deuterium oxide (D_2O) (Z99.9 atom% D) were also obtained from Aldrich. For EPR measurements, 5-Doxylstearic Acid (5-DSA) at 0.5 mM used as the spin probe**,** was obtained from Sigma.

Instruments and Methods

Cloud point (CP) determination: The measuring solution was taken in a securely stoppered thin glass test tube and placed in a heating mantle having arrangement for constant stirring and controlled increment of heat. The point of starting of clouding (turbidity) was visually observed and recorded. The heating was then stopped, and the system under stirring condition was allowed to cool slowly. The temperature for the disappearance of turbidity was also taken and the mean value of the two opposite directions was taken as the CP of the system. The experimental details were discussed in our previous reports.[24,25] The measured CP was accurate within ± 0.5K.

Isothermal Titration Calorimetry (ITC): For thermometric measurements, an OMEGA ITC microcalorimeter (Microcal, USA) was used. A concentrated solution of SDS (~325 μL in a microsyringe) was injected into 1.325 mL of solvent in the calorimetric cell at equal time intervals (210s) in multiple steps (32-50 additions) under constant stirring (350 rpm) condition. All measurements were taken under thermostated conditions maintained by a Nesleb RTE 100

circulating water bath. The heat released or absorbed at each step of dilution of surfactant solution in either water or polymer solution was recorded and the enthalpy change per mole of injectant was calculated by the ITC Microcal Origin 2.9 software. The reproducibility was checked from repeat experimentations. The procedures for the evalution of CMC and enthalpy of micellization (ΔH^0_m) were reported earlier.[24-27]

Nuclear Magnetic Resonance (NMR): NMR measurements were performed (at 298K) with the aid of ECA-500 JEOL FT-NMR spectrometer operating at 500 MHz. ^{1}H and ^{13}C chemical shifts, ^{1}H self-diffusion coefficients (D), ^{1}H spin-lattice relaxation times (T_1) and ^{1}H spin-spin relaxation times (T_2) were monitored for SDS/L31 (10 mM)/D_2O (system-I), SDS/ L31(50 mM)/D_2O (system-II), SDS (5 mM)/L31/D_2O (system-III) and SDS (50 mM)/ L31/D_2O (system-IV). Bipolar pulse pair longitudinal encode-decode (BPPLED) sequence[28] was used for the measurement of translational self-diffusion coefficients. The optimized experimental parameters like gradient duration (Ω) and diffusion time (Δ) were 6 ms and 200ms, respectively. The amplitude of the gradient (g) varied from 3 to 283 mT/m in 28 steps. A line broadening of 5 Hz was applied to each 'free-induction-decay' (FID) keeping in view of attaining a reasonable signal to noise ratio. The diffusion coefficients were extracted using nonlinear fitting of the experimental data to the following Stejaskal-Tanner equation,[29] $I = I_0 e^{-kD}$, where I_0 is the peak intensity in the absence of gradient pulses, and the parameter $k = (\gamma_n \Omega g)^2 (\Delta - \Omega/3)$ where, γ_n is the magnetogyric ratio and D is the translational self-diffusion coefficient. From the plots of intensity versus g^2, it was deduced that a single exponential nature of the magnetization recovery and the corresponding estimated error in D was about 5%. T_1 and T_2 measurements were carried out using inversion recovery and CPMG pulse sequences, respectively.[17] The observed magnetization recovery in both T_1 and T_2 data indicated the single-exponential decay and data

analysis were made using non-linear three and two-parameter fits, respectively. The errors encountered in both T_1 and T_2 fittings were less than 2%.

The ^1H and ^{13}C chemical shift measurements were made on SDS (97 mM)/L31/D_2O as a function of L31 for monitoring the preferential location of L31 in SDS. No internal reference was used in both ^1H and ^{13}C measurements. DSS in D_2O was used as an external reference, keeping the concentrations at 1 mM and 1 M for ^1H and ^{13}C Chemical shits, respectively. In ^1H /^{13}C spectra, the resonances were expressed relative to methyl protons/carbons of DSS, where their position was arbitrarily set as zero. Jeol-Delta-NMR software was used for all NMR data processing.

Electronic Spin Resonance (EPR): EPR measurements were taken using Bruker EMX computer-controlled spectrometer operating at X-band frequency with 100 kHz field modulation. A rectangular (ER 4102ST) universal cavity was used for the measurements. All measurements were performed at 295K. The microwave power and the modulation amplitude were kept constant for all measurements at 3 mW and 0.3 mT, respectively. It was reported that SDS micelle structure was not perturbed considerably if lower proportions of 5-DSA was used[9,30] and hence its concentration was fixed at a suitable value i.e., 0.5 mM in all EPR measurements. The preparation of the solutions containing the spin label (5-DSA) was made in the same way as found in the report.[9] The solutions were kept for 24h for equilibration and the EPR spectra were recorded after this period. The measurements were made using ER160FC-Q flat cell. The simulations of the EPR spectra were performed using Bruker Simphonia version 2.11 software package.

Small-Angle Neutron Scattering (SANS): Neutron scattering facility at DHRUVA reactor, Trombay, India was used for the SANS measurements. SANS data were recorded on

SDS/L31/D_2O mixtures as a function of both SDS and L31 concentrations (at 303K), where concentration of SDS and L31 kept fixed at 50 mM each. For obtaining good contrast in SANS experiments, D_2O was used as a solvent instead of H_2O. The incident wavelength utilized was 5.2 Å with $\Delta\lambda/\lambda$ = 15%. The scattering intensity was collected in the scattering vector (Q) range of 0.015–0.35 $Å^{-1}$. The SANS profiles were corrected for the background, the empty cell contributions, and the transmission, and converted to an absolute scale using standard protocols mentioned earlier.[17,23]

In SANS experiment, one measures the differential scattering cross section ($d\Sigma/d\Omega$) per unit volume as a function of Q and is expressed as[31]

$$\frac{d\Sigma}{d\Omega} = n(\rho_m - \rho_s)^2 V_m{}^2 P(Q)S(Q) + B \quad (1)$$

where n denotes the number density of the micelles, ρ_m and ρ_s are the scattering length densities of the micelle and the solvent, and V_m is the volume of the micelle, respectively. $P(Q)$ is the intraparticle structure factor and depends on the structure (shape and size) of micelles. $S(Q)$ is the interparticle structure factor and is decided by the correlation (interaction) of particles and B is the back ground constant. In our analysis, $P(Q)$ has been calculated using ellipsoidal micelles[32] and $S(Q)$ by the method of Hayter and Penfold for the screened Coulomb interaction between the charged micelles.[33,34] The composition of mixed micelle (volume and scattering length density) having x_1 and x_2 mole fractions of surfactant and polymer, respectively is modeled as[34]

$$V_m = N(x_1\nu_1 + x_2\nu_2) = N_1\nu_1 + N_2\nu_2 \quad (2)$$

$$\rho_m = x_1\rho_1 + x_2\rho_2 \quad (3)$$

where N_1 and N_2 are aggregation numbers, v_1 and v_2 are the monomer volumes, and ρ_1 and ρ_2 are the scattering length densities of surfactant and polymer, respectively. N (=N_1+N_2) represents to total aggregation number of the mixed micelle.

The data have been analyzed by the nonlinear least-squares fitting of the model scattering to the experimental data. Throughout the data analysis corrections were also made for instrumental smearing. The fitted data are given by the solid lines to the experimental data points. The fact that most of the scattering arise from the hydrophobic core region of the micelle, the scattering contribution from hydrated shell is neglected in the SANS data analysis.

3. Results and Discussion

Clouding behavior

The clouding is an effective way of understanding the phase behavior of pluronics in solution. The process is interpreted by temperature dependent dehydration of the PEO moiety (reduction of hydrogen bonding between ethereal oxygen of PEO and water), and polar-nonpolar conformation change of PEO.[35] The clouding process can be influenced by additives; both delay and enhancement were found.[36-41] The concentration dependent cloud points (CPs) of aqueous solutions of L31 ($E_2P_{16}E_2$) are presented in Fig. 1A. In this system, the PPO/PEO ratio is 4; thus clouding was easier, and the cloud point (CP) was 316K at 5 mM L31. The CP decreased exponentially from 316K (at 5 mM) to 301.5K at 100 mM following the relation: $CP = a + be^{-x/t_1}$, where a, b, t_1 are constants and x is the concentration of L31 (a = 28.68, b = 18.92, and t_1 = 17.22). SDS also influenced the CP of L31. The clouding behavior of L31 on SDS addition is presented in Fig. 1A (see inset). The nature of the dependence was much different from that of CP of L31, shown in Fig. 1A. Formation of separate phases of the components present in the solution of a compound or its mixture is considered as the threshold

point of clouding or the CP. It can be taken as the point of solubility limit of the material.[42] On this physicochemical basis, the energetics of the process can be evaluated. Equation 4 represents the standard Gibbs free energy change (ΔG_C^0), of clouding, where X_c is the concentration of L31 in mole fraction scale at the point of clouding. The enthalpy (ΔH_C^0), entropy (ΔS_C^0), and heat capacity ($\Delta C_{P,C}^0$) changes for the clouding process can be evaluated in the usual way and are described below.

$$\text{Thus, } \Delta G_C^0 = RT\ln X_C \quad (4)$$

Dependence of ΔG_C^0 on temperature has been used to get the enthalpy change of clouding (ΔH_C^0) by using a polynomial (eqn 5) as the plot was not linear (Fig. 1B). Since L31 was a nonelectrolyte, and the [SDS] used was in mM region, the activity of the solute system in solution was considered equivalent to its concentration.

$$\frac{\Delta G_C^0}{T} = A + \frac{B}{T} + \frac{C}{T^2} \quad (5)$$

$$\text{Thus, } \Delta H_C^0 = \frac{d\left(\Delta G_C^0/T\right)}{d(1/T)} = B + \frac{2C}{T} \quad (6)$$

with A, B, and C denoting the coefficients of the polynomial relation and T is the absolute temperature. The correlation coefficient of the fitting curve was 0.998.

From the knowledge of ΔH_C^0 dependence on temperature, the heat capacity of the clouding process was obtained from the eqn (7).[42,43]

$$\Delta C_{P,C}^0 = \frac{d\,\Delta H_C^0}{dT} \quad (7)$$

The results obtained are shown in Table 1. In the inset of the Fig. 1B, the linear plot between ΔH_C^0 and T is depicted to get $\Delta C_{P,C}^0$ of the process. Also, the compensation plot between ΔH_C^0

and ΔS_C^0 are depicted for the pure L31 system. The plot was nicely linear with a slope or the compensation temperature (T_C) equal to 308.4 K; the average temperature of the study was 306.6 K. The agreement was fair.

The ΔG_C^0 values of clouding were negative, whereas the ΔH_C^0 ΔS_C^0 values were both positive. For pluronic 85, endothermic ΔH_C^0 values were found by Prasad et al.[41] in the presence of hydrotopes. The athermal TX-100 ended up in high endothermic clouding, ΔH_C^0 (~ 50-1000 kJ mol^{-1}) in the presence of different proportion of saponin (acaciacide).[42] The clouding of salt induced PVP (polyvinyl pyrolidone) was reported to be in the range of ~140-350 kJ mol^{-1}.[24] In the present work, the behavior of SDS on clouding was quite different. However, with SDS, the ΔG_C^0, ΔH_C^0 and ΔS_C^0 values were all negative. Kabir-ud-din et al.[44] reported that in the presence of cationic surfactants (TTAB, DTAB, CTAB, and CPC), anionic surfactant (SDS), and gemini surfactants the clouding process of hydroxypropylmethyl cellulose was moderately endothermic (ΔH_C^0 = 4-20 kJ mol^{-1}). Thus the energetic parameters of pluronics and polymers alone and in presence of different additives are of different types. We may herein mention that positive ΔH_C^0 was also reported from DSC experiments on reverse pluronic 31R1;[45] and Naskar et al.[25] also reported it for 10R5. Influence on the clouding of polymer/water system by surfactants could be ascribed to the variation of the hydrophobic/hydrophilic balance in the system, which can cause modification of the interaction process.[44] The interaction of nonionic polymers with ionic surfactants formed a complex like a polyelectrolyte. Ionic head groups of the surfactant and the polar residues present in the polymer domains were responsible for the interaction[37,46] between the surfactants and the polymer, and in addition the hydrophobic interaction that arose from the forces between the nonpolar parts of both the entities. Fig. 1A evidenced an increase in CP by the addition of SDS in the system. At lower [L31], the trend was

nonlinearly upward, whereas at higher [L31] it was nonlinearly downward. So there existed a delicate balance between the electrostatic effect and hydrophobic interaction. At each [L31], SDS addition increased the CP. The rate of increase in CP at higher [SDS] for higher [L31] was less effective than that of lower [L31] with a trend of leveling out, whereas it was shooting up at much lower [L31]. The mechanism of the SDS effect on the phase separation process depended on the concentration of the aqueous solution of L31. Interestingly, the upward and downward trends in the curves were found to be grossly close to the CMC of the SDS (which were 9 mM at the CP values of 325, 313 and, 307 K, respectively).

Behavior of mixed SDS/L31 in aqueous medium

In this section, the behaviors of the mixed SDS and L31systems in different proportions in solution will be presented. The explored results found from microcalorimetry, NMR, EPR and SANS methods will be correlated and discussed in several subsections.

Microcalorimetric results: The dilution enthalpograms of SDS in water, and in 10 and 50 mM of L31 at 303K are presented in Fig. 2. SDS showed a sigmoidal type profile with inflection at CMC, and an exothermic standard enthalpy of micellization, $\Delta H_m^o = -2.46$ kJ mol^{-1}. The resultant enthalpograms of SDS interacted L31 minus the dilution enthalpy of SDS presented in the diagram showed inflections for CAC (critical aggregation concentration of polymer induced small micelle formation), and CMC_e (extended CMC which was greater than normal CMC without added polymer). The CAC and the CMC_e points are marked on the thermograms. These and their corresponding enthalpy values found**,** form the height differences in the enthalpograms are presented in Table 2. The standard Gibbs free energy changes ($\Delta G_C^0 = RT\ln X_{CAC}$ or X_{CMC_e}) and the computed entropy changes ΔS_{CAC}^0 and $\Delta S_{CMC_e}^0$ values (using the

relation $\Delta G^0 = \Delta H^0 - T\Delta S^0$) are also presented. From the data, the spontaneity of the processes and their associated energetics can be revealed.

NMR results

SDS diffusion in SDS/L31/D_2O mixtures: Fig. 3A and 3B depicted the diffusion co-effiecients of SDS and L31, respectively with increasing concentration of the former in A at a constant concentration of the other (i.e. L31) and vice versa. In A, the behavior of the pure SDS has been illustrated, the pattern of its self-association was sigmoidal with a distinct break at 7.76 mM**,** which is the CMC.[14] In 10 mM L31 microcalorimetry has shown a CAC at 2.0 mM of SDS, and a CMC_e at 8.7 mM. These regions are marked in Fig. 3A. The lighter entity SDS showed large changes in its D_{SDS} on interaction with L31, up to CAC and relatively less beyond this concentration. The heavier L31 had much lower D_{L31} which was lowered further away from CAC. In the post CMC_e region the diffusion coeffiecients of the similar mixed aggregates of L31-SDS declined exponentially. In Fig. 3B two sets of results at two [SDS] = 5 and 50 mM with variable addition of L31are presented. The diffusion values of SDS and L31 at 5 mM [SDS] are presented in the top two curves (symbols ■ and ●). As 5 mM SDS was > CAC (~ 2 mM), the inflection in the diffusion coefficient for CAC was absent but CMC_e region (8-10 mM, cf Figure 2) was observed. Thereafter, beyond 14 mM, both the D values (D_{SDS} and D_{L31}) continuously decreased because of clustering of both aggregates and increased medium viscosity. In the bottom two curves (symbols ▲ and ▼) results of L31 addition to 50 mM SDS are depicted. As 50 mM >> CMC_e of SDS, the assemblies were all SDS aggregates with which L31 interacted. The D_{SDS} and D_{L31} of the complexed species were more or less equal. The D_{L31} was marginally lower than the D_{SDS}. The trends again were found to continue up to 14 mM and then bifurcated (probably by way of some changes in the morphology) and again declined nearly merging with

the top courses mainly by the increased solution viscosity. SANS results (shown in a subsequent section) supported the above trends, and a model for SDS micelle-L31 has been proposed in scheme 1.

^{1}H spin-relaxation (R_2 and R_1) in L31/SDS systems: Nuclear spin-relaxation rates provide fruitful information on the slow and the fast dynamics in polymer-surfactant systems.[16,17] It is established that R_1 monitors the fast motions, and R_2 the fast as well as the slow motions. Hence, the difference in the relaxation rate ΔR (= R_2 - R_1) corresponded to the slow motions at the same frequency in the study.[16,47] In fact, ^{2}H relaxation study on the micelle systems can provide more reliable information on the fast and the slow dynamics over ^{1}H relaxation, as the latter involves contributions from the inter and the intramolecular interactions.[14,16] However, ^{1}H relaxation data convey both the fast and the slow dynamics at least in a qualitative way.[17] Hence, the ^{1}H relaxation rates for the SDS, PEO methylene and PPO methyl of the systems I-IV were monitored as a function of SDS/L31 concentration. Representative relaxation plots for the PPO methyl protons of the system-I as a function of the SDS concentration is shown in Fig. 3C. It was clear from the Fig. 3C that R_1 was insensitive to the SDS concentration in the experimental range of study, which reflected the fast motions. However, R_2 was sensitive to the concentration and resembled with ΔR (see Fig. 3C) indicating the predominance of the slow motions arising from the SDS-L31 mixed aggregates. The relaxation rates R_2 and R_1 of PPO-CH_3 with increasing [SDS] along with their differences $\Delta R = R_2$-R_1 values are presented in Fig. 3C. For R_2 and ΔR, the first decreased values matched with the CAC region and the second inflection tallied with the CMC_e region. Thus, the dynamics of the system as found in NMR study supported the physicochemical features produced by calorimetry in terms of sufactant polymer interaction.

^{1}H and ^{13}C NMR chemical shifts studies of SDS/L31/D_2O mixtures: ^{1}H and ^{13}C NMR spectra of SDS (97 mM)/D_2O and SDS (97 mM)/L31/D_2O systems were recorded at 298K, where L31 concentration was varied (from 5 to 200 mM) in the latter system. The ^{1}H and ^{13}C chemical shift assignments of the SDS, PPO and PEO were found elsewhere.[10,13,17] The ^{1}H and ^{13}C SDS chemical shifts for the SDS (97 mM)/L31/D_2O relative to the SDS (97 mM)/D_2O i.e., the values of the $\Delta\delta$ are plotted against SDS proton and carbon numbers presented in Fig. S1(ESI) and Fig. 3D, respectively. The SDS carbons C1, C2, C3, C10, C11 and C12 are presented for the analysis (see Fig. 3D), whereas other SDS carbons are precluded due to their tentative assignments. It was clear from the Fig. 3D that some of the SDS carbons experienced notable changes on changing the L31 concentration. The up-field $\Delta\delta$ trend and its increase with increase in L31 concentration, observed for SDS C1 carbon, indicated the adsorption and localization of the copolymer on the SDS micelle surface. However, the notable downfield shifts for the SDS C2 and C3 indicated the penetration of the copolymer up to C3. It may be noted that the ^{13}C downfield chemical shifts of the SDS alkyl chains was due to the guache-trans conformational changes.[48,49] It could be pointed out that the considerable downfield chemical shift of the C12 as a consequence of disparity in the chain length between the hydrophobic PPO and the SDS alkyl chain was also observed earlier.[17,48]

EPR results

For a better revelation of the polymer-surfactant interaction, we have also measured EPR rotational correlation time (τ_R) of a hydrophobic spin probe 5-DSA, which became located in the hydrophobic region of the mixed species of L31 and SDS in water.[9] EPR spectra of 5-DSA in SDS/H_2O (system-a) and 10mM L31/SDS/H_2O (system-b) are presented in Fig. S2 (ESI). It was

clear from Fig. 4A that the EPR line shape changes became prominent on changing the SDS concentration from 1 to 2 mM, with a noticeable line broadening due to the increased viscosity, signaling the formation of SDS-L31 mixed aggregates. The observed EPR lines were relatively narrow for the systems a and b which permited the analysis in the limit of fast motion. The EPR parameters A_N and τ_R were extracted using the simulation program.[9] The dependences of rotational correlation times (τ_R) of the spin probe in the systems a and b are shown in Fig. 4B. For a, the τ_R was constant in lower SDS concentrations (< 7 mM), while it started to increase from this concentration, signifying 7 mM as the CMC of SDS which well corroborated very well with the earlier EPR report.[9] In the EPR spectra of SDS/DSA/H_2O the 5-DSA produced three sharp line signals at low viscosity condition (like in water) before CMC;[9] in micellar environment (>8mM), the line widths of the peaks were broadened (supporting information) for hindered rotational mobility of the probe due to increased viscosity.[50] For the depiction 'b', a sudden increase in τ_R was observed at about 2 mM SDS (the CAC) and also the broadening of the line shape at the same concentration was observed (Fig. 4); a second inflection at 10 mM corresponded to CMC_e discussed earlier. The hyperfine coupling constants (A_N) were also measured for these systems, which gave information on the polarity of the spin-probe medium.[9] For pure SDS, in the concentration range of the study (4 - 40mM), the A_N values varied from 1.53 to 1.46 mT i.e., polar (unimer) to non-polar (micelle).[9] In system b, the changes in hyperfine coupling constant (see Table 3) were marginal indicating the presence of the polymer in the periphery of the L31-SDS mixed aggregates and not in the interior (cf. Scheme 1 in next section).

SANS results

SANS measurements were performed to get information on the microstructures of the assembled SDS/L31 sytems. The results taken on L31/D_2O (Fig. 5A) and SDS/L31/D_2O (Fig. 5B and 5C) as a function of [L31] and keeping the [SDS] fixed at 5 and 50 mM in B and C, respectively. Additional experiments were performed on SDS/L31/D_2O as a function of [SDS] at a fixed [L31] 50 mM (Fig. 5D). For L31/D_2O the SANS profiles exhibited features pertaining to associating liquids.[51] The data were fitted to Gaussian distribution of L31 unimers.[51] The R_g was found to be insensitive to [L31] (Table 4), which indicated inability of L31 to form micelles/aggregates. But in the presence of 5 mM SDS, L31/D_2O encountered differential behavior (Fig. 5B) relative to SDS-free situation (Fig. 5A). There was an overall increase in the scattering as well as contribution of the structure factor indicating the association of the L31 in the presence of SDS.

The results presented in Table 4 represent prolate ellipsoidal mixed aggregates/micelles comprising SDS and L31, and the size increased with [L31]. The SDS aggregation number (N_{SDS}) was too low (~3) compared to the conventional micelles (N_{SDS} ~ 60), whereas the aggregation tendency of the L31 changed noticeably manifested as an increase in the aggregation number of the L31 (N_{L31}) from 8 to 20 (Table 4). The mixed micelles were rich in L31. The fractional charge (α) in the micelles increased from 0.57 to 0.93 as a consequence pointed out the lowering of surface charge density of the mixed aggregates with increasing [L31] (Table 4). The SANS intensity profiles for 50mM SDS/L31/D_2O (Fig. 5C) were similar to that of 5mM SDS/L31/D_2O (Fig. 5B) but was pronounced due to higher [SDS]. The data showed a correlation peak of the structure factor whose position ($Q_p \sim 2\pi/d$, where d is the distance between micelles) was decided by the distance between the mixed micelles. This distance depended on the size and composition of the mixed micelle.[23] The results of the analysis are

documented in Table 4. The data revealed prolate ellipsoidal geometry of the mixed aggregates, whose size was sensitive to the composition ratio, and increased with [L31]. In the mixed aggregates, N_{SDS} decreased from 34 to 18, and N_{L31} increased from 7 to 68 (Table 4). The presence of SDS (50 mM) in the aggregated species made α to increase from 0.39 to 0.8. The SANS profiles for SDS/50 mM L31/D_2O as a function of SDS concentration showed tendency of shifting towards higher Q values with intensity change (Fig. 5D) relative to that in Figure 5C. In the prolate ellipsoidal mixed aggregates N_{SDS} increased from 2 to 35 whereas the N_{L31} decreased from 20 to 9 with increasing presence of the former (Table 5). As a consequence, α decreased from 0.93 to 0.36.

With reference to Table 4, it may be concluded that in SDS/L31/D_2O system at 5 mM SDS with increasing [L31] from 10 to 30 mM moderately increased the aggregate axial ratio (a/b) from 3.6 to 4.3. At 50 mM SDS, varying [L31] increased the prolate geometry (a/b) from 1.88 to 3.55 for [L31] = 10 to 90 mM wherefrom it decreased to 3.07 at [L31] = 200 mM. A contrasting situation arose for the system SDS/50 mM L31/D_2O as a function of [SDS], where a/b decreased from 4.3 to 1.9 (Table 5). In the process, the semimajor axis decreased whrereas the semiminor axis increased, and the rate of change of 'a' was more than that of 'b'. Effectively, the prolate geometry tended to expand towards globules. In the overall perspective, the prolate to near prolate micellar aggregates wrapped around by the pluronic molecules (supported by ^{13}C chemical shift data in Fig. 3D) were energetically favourable to avoid contact with water. A probable model of such elliptical assemblies is depicted in the Scheme 1.

4. Conclusions

The self-aggregation dynamics and microstructure of SDS influenced by the L31 in aqueous medium was investigated from CP, ITC, NMR, EPR and SANS measurements. The energetics of the clouding phenomenon were evaluated, the process being exothermic, thus helped to stabilize L31 in solution by way of molecular complex formation between polymer and SDS. The ITC, NMR and EPR data revealed the synergistic effect between SDS and L31 manifesting an early induced small micelle formation i.e. CAC (~ 2mM) leading to an extended critical micelle formation, called CMCe (~ 10 mM) of SDS. The formation of spheroidal SDS micelles with peripherial L31 coverage was envisaged (scheme 1). The marginal decrease in the ^{14}N hyperfine coupling constants of 5-DSA indicates the preferential location of L31 near the SDS micellar surface, which well corroborated with ^{13}C NMR chemical shift results.

The SANS analysis indicated that aqueous L31 did not form micelles in the concentration range of study (upto 200 mM). However, L31 in the presence of SDS monomers (5 mM) could induce prolate ellipsoidal mixed aggregate formation with a persistent axial ratio (~ 4). An order of increase in SDS concentration (5 to 50 mM) promoted the size of the mixed aggregates and changed the shape from nearly spherical to non-spherical (ellipsoidal). On the other hand, shape evaluation of mixed aggregates from non-spherical (ellipsoidal) to nearly globular was observed for L31 (fixed at 50 mM) upon increasing the SDS concentration in the mixture. L31-rich and SDS-poor and SDS-rich and L31-poor mixed aggregates were found with increase in L31 and SDS concentrations, respectively. Hence, by a judicious choice of the L31 to SDS ratio, the formation of different morphologies of mixed micelles ranging from globular to ellipsoidal could be achieved, which might find applications (1) in controlled-drug delivery as nano-carriers, and (2) templates for the preparation of nano-structured materials.

Acknowledgements

G. K. S. P thankful for DST Women Scientist Scheme-A Fellowship. The use of the NMR facility at CSIR-CLRI is gratefully acknowledged. The authors (B. V. N. P. K and A. B. M) would also like to acknowledge the support from the STRAIT project under the XII five year plan of CSIR-CLRI. A. P. thankful to UGC, government of India, New Delhi, for Senior Research Fellowship and S. P. M thanks Jadavpur University and Indian National Science Academy for the positions of Emeritus Professor and Honorary Scientist, respectively.

Supporting Information Available

Fig. S1 illustrates ^{1}H chemical shifts of SDS for SDS (97 mM) / L31/ D_2O relative to SDS and the EPR experimental and simulated spectra of the spin probe 5-DSA are documented in Fig. S2.

References

1. J. C. Brackman and J. B. F. N. Engberts, *Chem. Soc. Rev.*, 1993, **22**, 85-92.

2. P. Alexandridis and T. A. Hatton, *Colloid Surf. A: Physicochem., Eng. Aspects,* 1995**, 96**, 1-46.

3. G. Wanka, H. Hoffmann and W. Ulbricht, *Macromolecules,* 1994, **27**, 4145-4159.

4. K. C. Tam and E. Wyn-Jones, *Chem. Soc. Rev.,* 2006, **35**, 693-709.

5. S. Courdec, J. Sidhu, T. Thurn, R. Xu, D. M. Bloor, J. Penfold, J. F. Holzwarth and E. Wyn_Jones, *Langmuir,* 2005, **21**, 10197-10208.

6. J. R. Lopes and W. Loh, *Langmuir,* 1998, **14**, 750-756.

7. S. Senkow, S. K. Mehta, G. Douhe´ret, A. H. Roux and G. Roux-Desgranges, *Phys. Chem. Chem. Phys.,* 2002, **4**, 4472–4480.

8. S. Senkov, A. H. Roux and G. Roux-Desgranges, *Phys. Chem. Chem. Phys.,* 2004 , **6** , 822-828.

9. P. Deo, S. Jockusch, M. F. Ottaviani, A. Moscatelli, N. J. Turro and P. Somasundaran, *Langmuir,* 2003, **19***,* 10747-10752.

10. B. Cabane, *J. Phys. Chem.,* 1977, **81**, 1639-1645.

11. E. Petterson, D. Topgaard, P. Stilbs and O. Söderman, *Langmuir*, 2004, **20**, 1138-1143.

12. M. I. Gjerde, W. Nerdal and H. Hoiland, *J. Colloid Interface Sci.,* 1998, **197**, 191-197.

13. S. Barhoum and A. Yethiraj, *J. Chem. Phys.,* 2010, **132**, 024909.

14. B. V. N. Phani Kumar, U. S. Priyadharsini, G. K. S. Prameela and A. B. Mandal, *J. Colloid Interface Sci.,* 2011, **360**, 154-162.

15. P. Vangeyte, B. Leyh, L. Auvray, J. Grandjean, A.-M. Misselyn-Bauduin and R. Jerome, *Langmuir,* 2004, **20**, 9019-9028.

16. S. Abrahmsen- Alami and P. Stilbs, *J. Phys. Chem.,* 1994, **98**, 6359-6367.

17. G. K. S. Prameela, B. V. N. Phani Kumar, V. K. Aswal and A. B. Mandal, *Phys. Chem. Chem. Phys.*, 2013, **15**, 17577-17586.

18. J. Zhao and B. M. Fung, *Langmuir,* 1993, **9**, 1228-1231.

19. P. -G. Nilsson and B. Lindaman, *J. Phys. Chem. B,* 1984, **88**, 5391-5397.

20. P. J. Bratt, D. G. Gillies, L. H. Sutcliffe and A. J. Williams, *J. Phys. Chem.,* 1990, **94**, 2727-2729.

21. M. Jansson, P. Li and P. Stilbs, *J. Phys. Chem.,* 1987, **91**, 5279-5286.

22. J. James, S. Vellaichami, R. S. G. Krishnan, S. Samikannu and A. B. Mandal, *Chem. Phys*., 2005*,* **312**, 275-287.

23. R. Ganguly, V. K. Aswal, P. A. Hassan, I. K. Gopalakrishnan and S. K. Kulshreshtha, *J. Phys. Chem.,* 2006, **110**, 9843-9849.

24. A. Dan, S. Ghosh and S. P. Moulik, *J. Phys. Chem. B,* 2008, **112**, 3617-3624.

25. B. Naskar, S. Ghosh and S. P. Moulik, *Langmuir,* 2012, **28**, 7134-7146.

26. A. Pan, S. S. Mati, B. Naskar, S. C. Bhattacharya and S. P. Moulik, *J. Phys. Chem. B,* 2013, **117**, 7578-7592.

27. A. Pan, B. Naskar, G. K. S. Prameela, B. V. N. Phani kumar, V. K. Aswal, S. C. Bhattacharya, A. B. Mandal and S. P. Moulik, *Soft Matter,* 2014, **10**, 5682-5694.

28. D. H. Wu, A. D. Chen and C. S. Johnson, *J. Magn. Reson., Ser. A,* 1995, **115**, 260-264.

29. E. O. Stejskal and J. E. Tanner, *J. Chem. Phys.,*1965, **42**, 288-292.

30. A. M. Wasserman, M. V. Motyakin, L. L. Yasina, Y. A. Zakharova, V. N. Matveenko, Y. V. Shulevich and L. Z. Rogovina *Appl Magn Reson.,* 2010, **38**, 117–135.

31. J. B. Hayter and J. Penfold, *Colloid Polym. Sci.,* 1983, **261**, 1022–1030.

32. J. S. Pedersen, *Adv. Colloid Interface Sci.,* 1997, **70**, 171–210.

33. S. De, V. K. Aswal, P. S. Goyal and S. Bhattacharya, *J. Phys. Chem. B*, 1997, **101**, 5639–5645.

34. J. B. Hayter and J. Penfold, *Mol. Phys.,* 1981, **42**, 109–118.

35. M. Almgren, W. Brown and S. Hvidt, *Colloid Polym. Sci.,* 1995, **273**, 2-15.

36. H. Scott, *J. Colloid Interface Sci.,* 1997, **192**, 458-462.

37. G. Karlstrom, A. Carlsson and B. Lindman, *J. Phys. Chem.,* 1990, **94**, 5005-5015.

38. D. Varade, R. Sharma, V. K. Aswal, P. S. Goyal and P.Bahadur, *Eur. Polym. J.,* 2004, **40**, 2457-2464.

39. S. Saito, *J. Colloid Interface Sci.,* 1967, **24**, 227-234.

40. Z. –J. Yu and G. Xu, *J. Phys. Chem.,* 1989, **93**, 7441-7445.

41. M. Prasad, S. P. Moulik, D. Chisolm and R. Palepu, *J. Oleo. Sci.,* 2003, **52**, 523-527.

42. P. R. Majhi, K. Mukherjee, S. P. Moulik, S. Sen and N. P. Sahu, *Langmuir,* 1999, **15**, 6624-6630.

43. M. Prasad, S. P. Moulik, A. Al. Wardian, S. Moore, A. van Bommel and R. Palepu, J. Colloid Polym Sci., 2005, 283, 887-897.

44. N. Sardar, M. S. Ali, M. Kamil and Kabir-ud-Din, *J. Chem. Eng. Data,* 2010, **55**, 4990-4994.

45. P. A. Galera-Gomez and T. Gu, *Langmuir*, 1996, **12**, 2602-2604.

46. S. Ghosh and S. P. Moulik, *Indian J. Chem.,* 1999, **38A**, 10-16.

47. A. Ceglie, G. Colafemmina, M. D. Monica, U. Olsson and B. Joensson, *Langmuir*, 1993, **9**, 1449-1455.

48. N. Almgren, J. V. Stam, C. Lindblad, P. Li, P. Stilbs and P. Bahadur, *J. Phys. Chem.,* 1991, **95**, 5677-5684.

49. A. Pan, B. Naskar, G. K. S. Prameela, B. V. N. Phani Kumar, A. B. Mandal, S. C. Bhattacharya and S. P. Moulik, *Langmuir*, 2012, **28**, 13830−13843.

50. M. F. Ottaviani, R. Daddi, M. Brustolon, N. J. Turro and D. A. Tomalia, *Appl. Magn. Reson.,* 1997, **13**, 347-363.

51. P. Debye, *J. Phys. Colloid Chem.*, 1947, **51**, 18–32.

Figure Captions

Fig. 1: (A): Concentration dependent clouding behavior of L31, Inset: Effect of [SDS] on clouding behavior of L31 at different concentration; (B): $(\Delta G_C / T)$ vs (1/T) plot for the determination of ΔH_C, Inset: variation of ΔH_C with temperature and compensation plot between ΔH_C and ΔS_C.

Fig. 2: Enthalpogram of SDS dilution in water and L31 at 303K, Transition points are indicated in the diagram.

Fig. 3: (A): Variable SDS concentration self-diffusion profiles for SDS and L31 for the system SDS/L31 (10 mM)/D_2O. Self-diffusion data of SDS/D_2O is also given for the sake of comparison. (B): Variable L31 concentration self-diffusion profiles for SDS and L31 for the systems SDS (5 mM)/L31/D_2O and SDS (50 mM)/L31/D_2O. (C): Variable SDS concentration spin-relaxation profiles for the system SDS/L31(10mM)/D_2O. (D): ^{13}C chemical shifts of SDS for SDS (97 mM) / L31/ D_2O relative to SDS (97 mM)/ D_2O i.e. $\Delta\delta$ ($= \delta_{L31+SDS} - \delta_{SDS}$) as a function of L31 concentration.

Fig. 4: (A): EPR line shapes for (i) 1 mM and (ii) 2 mM SDS for the system 10mM L31/ SDS/Water. The dotted and solid lines represent the simulated and experimental spectra, respectively. (B): Rotational correlation times (τ_R) of the EPR spin probe 5-DSA for the systems-a and b.

Fig. 5: SANS profiles of (A): L31, (B): 5 mM SDS and (C): 50mM SDS in D_2O, as a function of L31 concentration, and (D): 50mM L31 against SDS concentration.

Scheme 1: Proposed microstructures for SDS-L31 in terms of spherical and prolate ellipsoidal mixed aggregates at different SDS/L31 compositions.

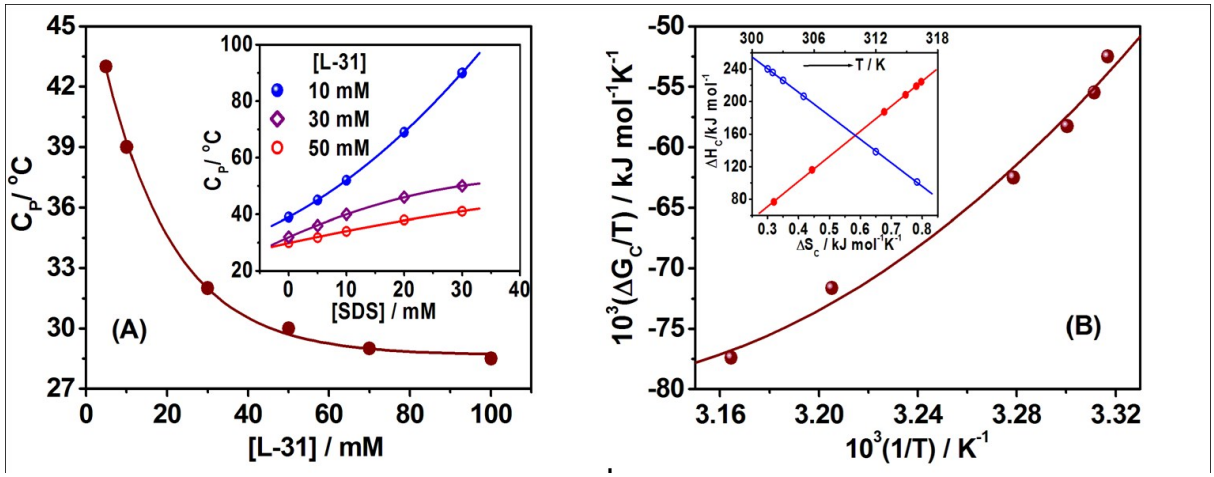

Fig. 1:

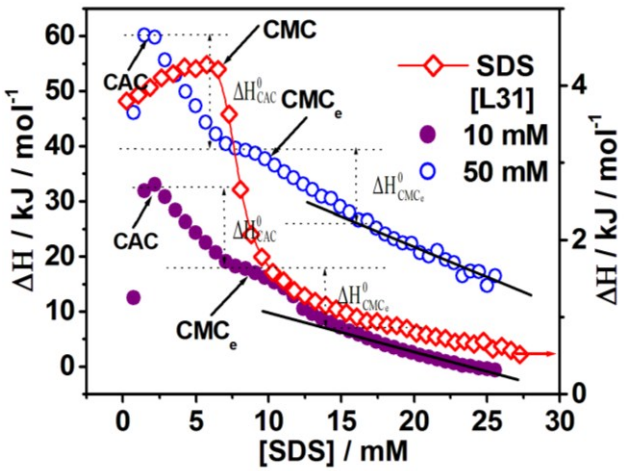

Fig. 2:

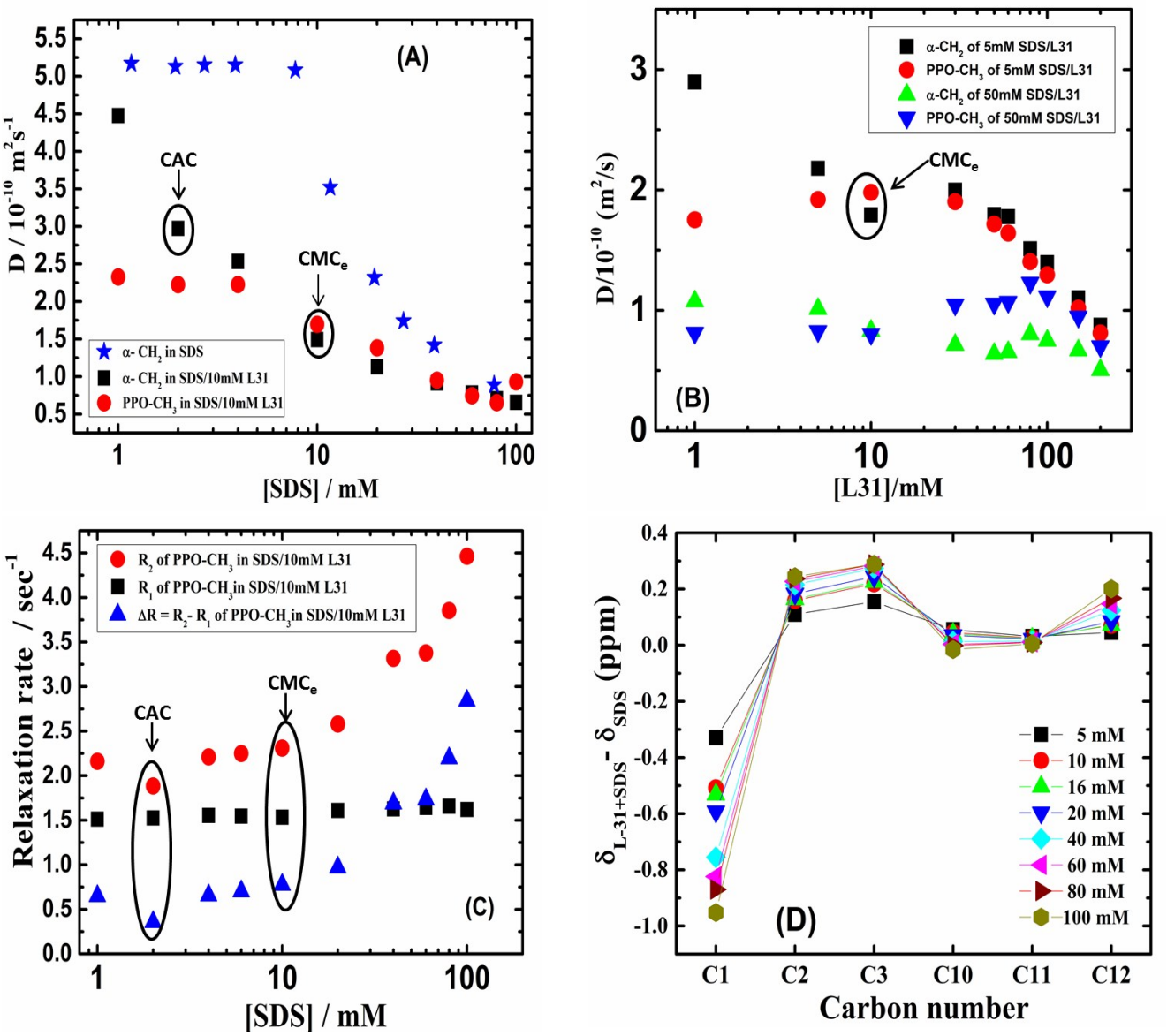

Fig. 3:

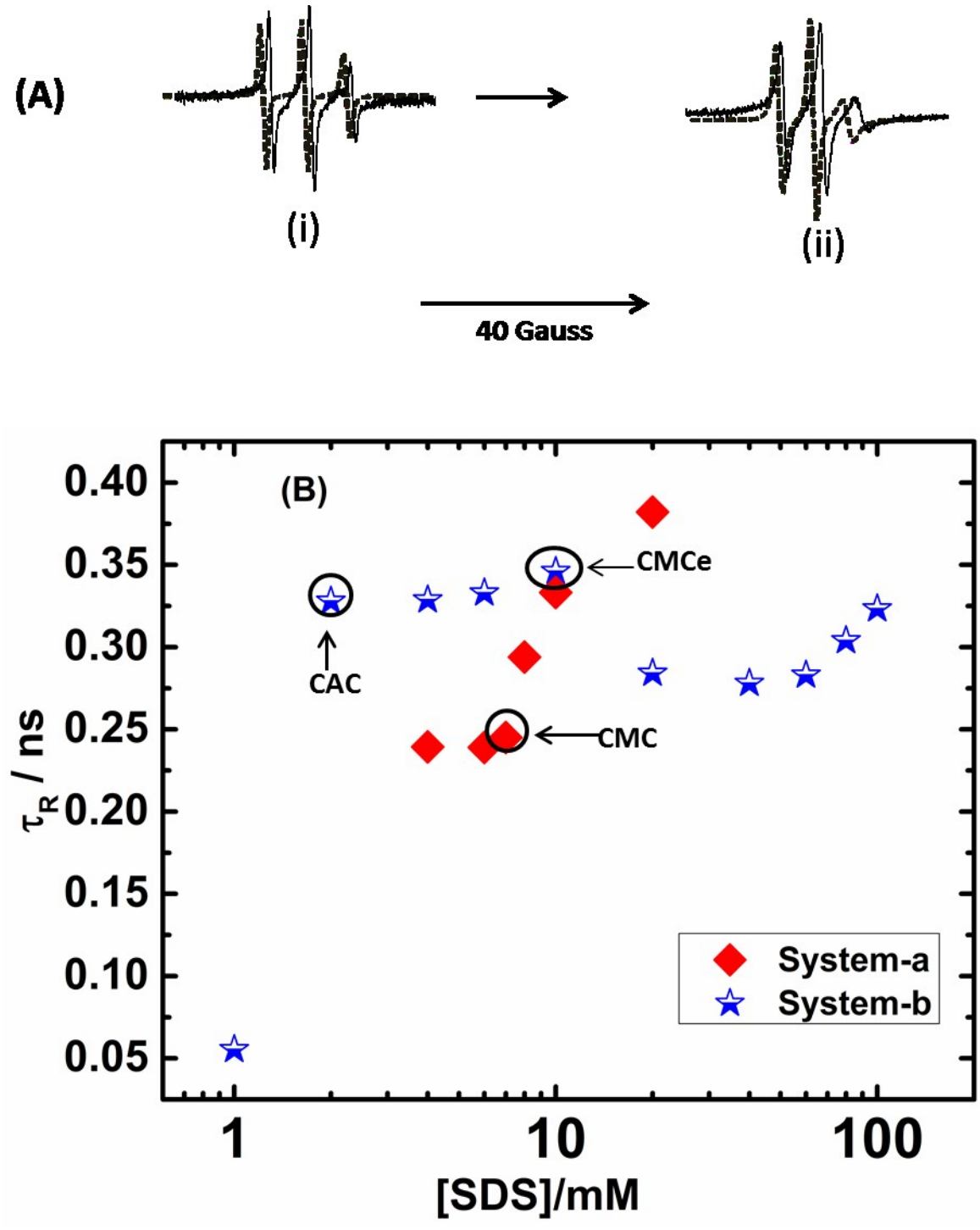

Fig. 4:

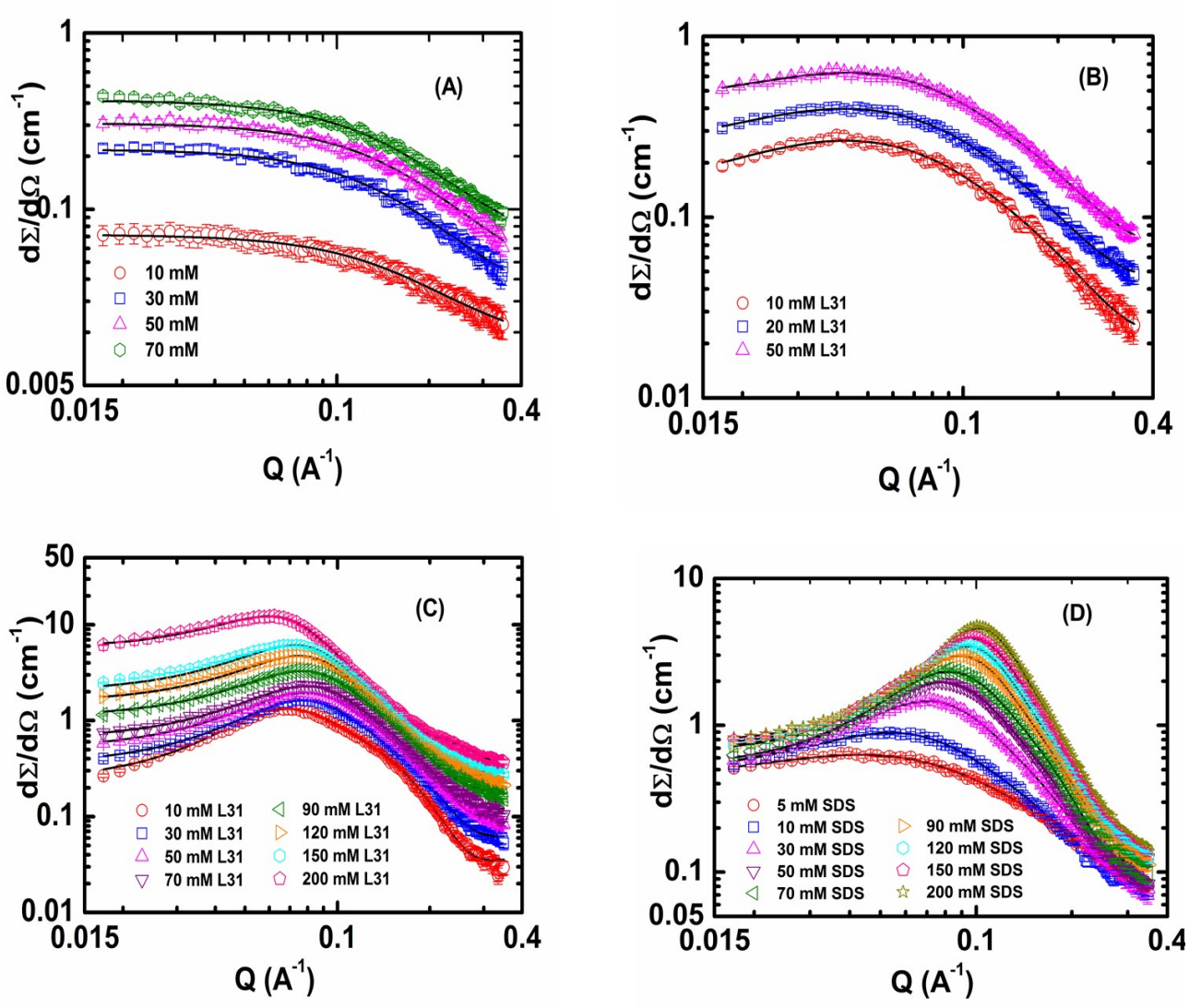

Fig. 5:

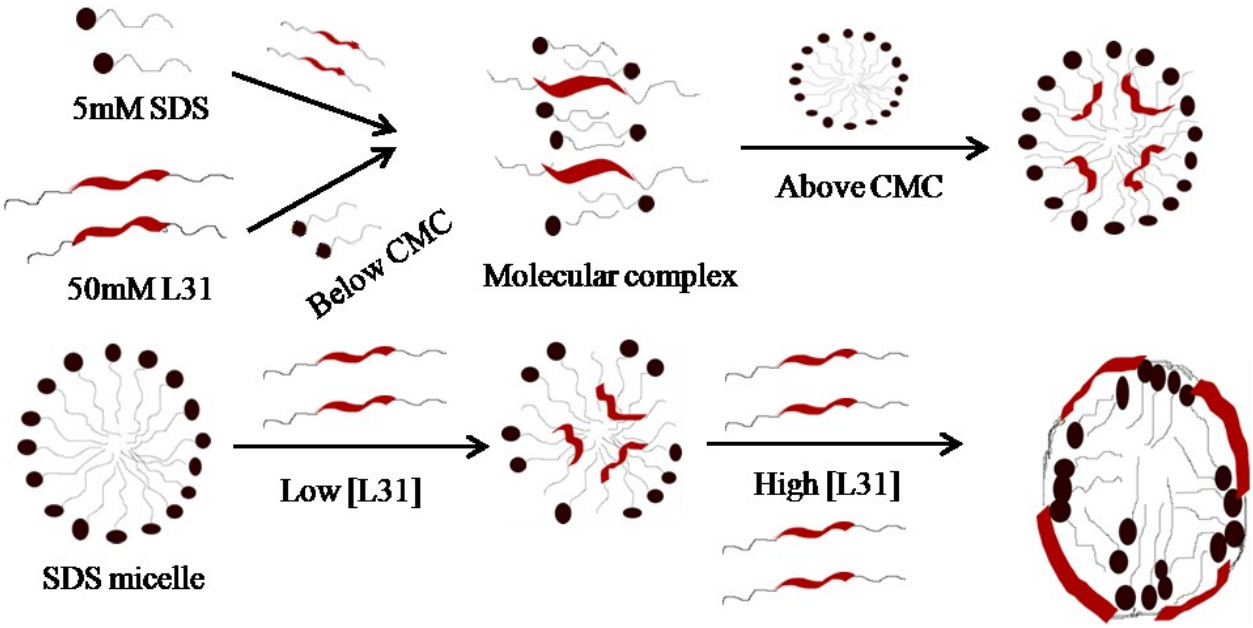

Scheme 1: Proposed microstructures for SDS-L31 in terms of spherical and prolate ellipsoidal mixed aggregates at different SDS/L31 compositions.

Table 1: Energetics of clouding of pluronic L31 and in presence of SDS in aqueous media.

Section (A)				
[L31]/mM	CP/K	ΔG_C^0 /kJ mol^{-1}	ΔH_C^0 /kJ mol^{-1}	ΔS_C^0 /kJ mol^{-1} K^{-1}
5	316	-24.5	101.2	0.32
10	312	-22.4	138.4	0.44
30	305	-19.1	206.5	0.68
50	303	-17.7	226.1	0.75
70	302	-16.8	235.8	0.78
100	301.5	-15.8	240.2	0.80

Section (B)												
	CP/K			ΔG_C^0 /kJ mol^{-1}			ΔH_C^0 /kJ mol^{-1}			ΔS_C^0 /kJ mol^{-1} K^{-1}		
[SDS]/mM	[L 31]/mM											
	10	30	50	10	30	50	10	30	50	10	30	50
5	318	309	304.8	-24.6	-23.9	-23.6	-72.5	-142.1	-237.5	-0.15	-0.38	-0.70
10	325	313	307	-23.3	-22.4	-22.0	-60.1	-120.0	-195.2	-0.11	-0.31	-0.56
20	342	319	311	-22.5	-21.0	-20.5	-31.9	-87.9	-119.8	-0.03	-0.21	-0.32
30	363	323	314	-22.6	-20.2	-19.6	-0.82	-67.2	-64.6	0.06	-0.14	-0.14

Table 2: Interaction and thermodynamic parameters of L31-SDS in aqueous medium at 303K [a].

[L31]/mM	Microcalorimetry			
	CAC/CMC_e	$\Delta G_{CAC}^0 / \Delta G_{CMC_e}^0$	$\Delta H_{CAC}^0 / \Delta H_{CMC_e}^0$	$\Delta S_{CAC}^0 / \Delta S_{CMC_e}^0$
10	2.07/8.76	-25.7/-22.0	-14.8/-10.9	35.9/36.6
50	1.82 / 10.2	-26.0/-21.7	-20.7/-13.2	17.5/28.1

[a] ΔG^0, ΔH^0, and ΔS^0 are expressed in kJ mol^{-1}, kJ mol^{-1}, and J mol^{-1} K

Table 3: EPR parameters* obtained from simulation of the experimental data for SDS/L31/H_2O as a function of SDS concentration (at 295K).

[SDS]/mM	SDS/H_2O		[SDS]/mM	[L31] /10mM	
	A_N	τ_R		A_N	τ_R
4	1.53	0.239	1	1.525	0.055
6	1.51	0.239	2	1.485	0.328
7	1.44	0.245	4	1.475	0.329
8	1.47	0.294	6	1.48	0.333
10	1.47	0.333	10	1.48	0.346
20	1.425	0.382	20	1.465	0.284
40	1.465	-	40	1.465	0.278
			60	1.465	0.283
			80	-	0.304
			100	1.475	0.323

*A_N and τ_R are expressed in the units of mT and ns, respectively.

Table 4: Fitted SANS parameters* for SDS/L31/D_2O as a function of L31 concentration (at 303K).

[L31]/ mM	[SDS] (0 mM)	[SDS] (5 mM)					[SDS] (50 mM)				
	R_g	a	b=c	N_{SDS}	N_{L31}	α	a	b=c	N_{SDS}	N_{L31}	α
10	10.7	36.2	9.6	4	8	0.57	26.8	14.2	34	7	0.39
20		40.5	10.1	3	12	075	-	-	-	-	-
30	10.9	50.7	11.8	2	20	0.93	33.1	13.7	20	12	0.52
50	10.5	-	-	-	-	-	39.5	13.7	16	16	0.55
70	10.8	-	-	-	-	-	46.1	13.9	15	21	0.60
90		-	-	-	-	-	50.8	14.3	14	25	0.65
120		-	-	-	-	-	52.3	16.1	14	34	0.71
150		-	-	-	-	-	54.5	17.9	15	45	0.76
200		-	-	-	-	-	62.7	20.4	18	68	0.80

*R_g, a, b and c are expressed in Å.

* At 5 mM SDS, (a/b) ratios for 10, 20, and 30 mM of L31 are 3.8, 4.1, 4.3, respectively.

Table 5: Fitted SANS parameters* for SDS/L31/D_2O as a function of SDS concentration (at 303K).

[SDS]/mM	[L31]/50mM					
	a	b=c	(a/b)	N_{SDS}	N_{L31}	α
5	50.7	11.8	4.3	2	20	0.93
10	46.5	12.7	3.7	4	20	0.85
30	41.6	13.0	3.2	11	18	0.64
50	39.5	13.7	2.9	16	16	0.55
70	36.3	13.9	2.6	20	14	0.50
90	31.7	14.2	2.2	22	12	0.46
120	29.8	14.5	2.1	26	11	0.43
150	29.1	14.5	2.0	30	10	0.40
200	28.2	14.7	1.9	35	9	0.36

*a, b and c are expressed in Å.